



Systematic studies of the structural, optoelectronic and thermoelectric characteristics of Hafnium based zintl HfCu₂X₂ (X= N, P, As, Sb and Bi) compounds

Zeshan Zada^a, Abdul Munam Khan^b, Ali H. Reshak^{c,d,e,*}, Abdul Ahad Khan^f, Dania Ali^g, Muhammad Irfan^h, Rabail Bibiⁱ, Muhummad Ismailⁱ, Amel Laref^j, Muhammad Ismail^k, Muhammad M. Ramli^e

^a Materials Modeling Lab, Department of Physics, Islamia College University, Peshawar, 25120, Pakistan

^b Department of Physics, RIPHAH International University Lahore, Lahore, Pakistan

^c Physics Department, College of Science, University of Basrah, Basrah, post code 61004, Iraq

^d Department of Instrumentation and Control Engineering, Faculty of Mechanical Engineering, Czech Technical University in Prague, Technicka 4, Prague 6 166 07, Czech Republic

^e Center of Excellence Geopolymer and Green Technology (CEGeoGTech), University Malaysia Perlis, 01007, Kangar, Perlis, Malaysia

^f School of Engineering and Built Environment, Gold Coast Campus, Griffith University, QLD 4222, Australia

^g Faculty of Medicine, Charles University, Pilsen, 30100, Czech Republic

^h Department of Physics, University of Sargodha, Sargodha, Punjab, Pakistan

ⁱ Department of Chemistry, Women University Swabi, KP, Pakistan

^j Department of Physics and Astronomy, College of Science, King Saudi University, Riyadh, 11451, Saudi Arabia

^k School of Environment and Chemical Engineering, North China Electric Power University, Beijing, 102206, PR China

ARTICLE INFO

Keywords:

Hafnium based zintl
Thermoelectric
DFT
BoltzTrap

ABSTRACT

By using first principles calculations the structural, optoelectronic and thermal properties of HfCu₂X₂ (X = N, P, As, Sb, Bi) belong to Zintl family are calculated via WIEN2K code. The volume of the unit cell is optimized at ground state by including modified Becke-Johnson (mBJ) potential. HfCu₂X₂ Zintl phase shows metallic behavior due to overlapping in between high symmetry $\Gamma \rightarrow K$ and $\Gamma \rightarrow M$ points and missing gap behavior between conduction and valence band. In TDOS, the major participation is due to copper (Cu) followed by Hafnium (Hf) and (X) elements, while in PDOS the strong hybridization for the necessary electrical transportation between Cu-d of valence and (Hf-d and X-p) states of conduction bands is observed for the current studies. The attributes of optical are calculated via dielectric function such as real/imaginary parts with other optical constants like refractive index, absorption etc. The maximum reflection throughout occurs in the HfCu₂Bi₂ compound, while HfCu₂Sb₂ has the highest extinction coefficient, which indicates that it absorbs more photons than the others. Further evidence that all these materials are excellent absorbers and promising new candidates for high range frequency-energy optical devices. By using BoltzTrap transport theory, thermoelectric response of the Hf-based materials is investigated and reported between temperature range from 0 to 800 K. It can be seen that HfCu₂As₂ compound shows higher value of ZT that is 1.1 followed by HfCu₂N₂ and HfCu₂Bi₂ with values (1 and 0.9) at 50 K temperature. Further the compound HfCu₂As₂ depicts (n-type) while HfCu₂Bi₂ shows (p-type) nature due to the presence of Seebeck curves in these negative/positive regions within 50–550 K temperature range. Materials with strong thermoelectric capabilities are generally found in high reflectivity zones and potentially effective in preventing solar heating.

1. Introduction

The word inter-metallics is mainly not explored and various

combination of metals that makes inter-metallic compound were found. Although many of these have been organized completely based on crystal structure and physical properties, but structural applications of

* Corresponding author. Physics Department, College of Science, University of Basrah, Basrah, post code 61004, Iraq.

E-mail address: maalidph@yahoo.co.uk (A.H. Reshak).

inter-metallics have been unexplored yet due to their high structural stability and low fracture toughness of materials at the surrounding temperature [1]. Apart from this, many inter-metallics compounds have been widely studied because of their practical applications in numerous areas like optoelectronics, spintronics and thermoelectric [2]. Intermetallic compound having AM_2X_2 -type formula, where A refers to rare earth element, M is a metal and X belongs to main group III, IV or V of the periodic table. The explorer of novel thermoelectric materials has obtained very fast improvement in last few decades as thermoelectric technology provides the dormant for environmentally friendly and continuous energy conversion procedure from waste heat to electricity without releasing any toxic or harmful waste. The Zintl families [3] have accumulated a significant amount of attraction for their capability as high achievement in thermoelectric research industry, both theoretically and experimentally. Zintl phase compounds are belong to AB_2X_2 family. 'A' refers to the Alkaline earth metals and 'B' represent the transition metals. Zintl compounds include, $Mg_{3+\delta}(Sb/Bi/Te)_2$ and $Yb(Cd/Zn)_2Sb_2$ have been ZT values ($ZT > 1$), other Zintl phases like $BaCuS_2$ and $CaAl_2Si_2$ are described with excessive ZT within available literature, mainly $CaZn_2Si_2$ having ZT greater than one for both n/p type compounds. These well-functioning thermoelectric materials are utilized for multivalley electronic band structure. The capability of thermoelectric devices (TE) is determined by the TE figure of merit ZT [4].

As, $ZT = \frac{\sigma S^2}{K} T$; where σ represents (electrical conductivity), S represents (Seebeck coefficient) [5], T shows the absolute-temperature and K represent (thermal conductivity). In thermoelectric devices, high figure of merit (ZT) [6] and Carnot efficiency [7] are the major features. Absolute temperature 'T' and Seebeck coefficient have great influence on 'ZT' values as performing electrical/thermal conductivity. An exceptional performance of thermoelectric devices can be achieved by high Seebeck coefficient, high electron mobility and low thermal conductivity. In spintronics, optoelectronic generator and electronic devices, zintl phases are also extensively used except their use in different thermoelectric applications [8,9].

The capacity of a material to efficiently conduct electricity, to allow electron-transfer to occur, and to withstand high heat for an extended period of time are the main characteristics that has to be taken into account from a material when creating a thermoelectric property. Only materials that can meet these criteria can be expected to produce a good outcome [10–14]. The productivity of heat conversion to electricity from the thermoelectric framework will increase with increasing ZT material estimation [15–18].

Equation shows that desirable thermoelectric properties include high electrical conductivity, a big Seebeck coefficient for maximum conversions of heat to electric power and cooling performance, and low heat conductivity to prevent heat from passing through the material [19]. The Seebeck thermoelectric effect is the direct transformation of heat energy into electrical energy or vice versa as a result of a material's temperature difference. The material for the thermoelectric generator is a semiconductor of the type P, which requires electrons (holes), and the type N, which has an abundance of electrons [20,21].

The Seebeck coefficient, which is a property of the material, is expressed by equation $S = \frac{\Delta V}{\Delta T}$ and indicates the rate of progressive change between the thermoelectric voltage (E) and (T). The thermoelectric module's characteristics are greatly influenced by the value of Seebeck coefficient. The (ZT) value will be calculated using this Seebeck coefficient value [22]. Additionally, materials with excellent TE characteristics are in high demand because they may be used as a replacement source to recycle waste heat from large enterprises and automobiles [23,24]. By converting waste heat, devices reliant on these materials may be used to generate electricity [25].

This technique has great promise for dealing with environmental problems on a worldwide scale and recovering waste heat. In light of the thermoelectric effect, the direct conversion of heat energy to electricity has long piqued the interest of material physicists [26]. We must

examine the thermoelectric characteristics in order to appreciate the component at play and improve the TE properties of materials. Due to their high interdependence, the three crucial factors cannot be changed separately [27]. As a result, material scientists are searching for novel materials with improved thermoelectric performance and higher ZT estimates.

Since there is currently a lack of theoretical or computational information on the Hafnium (Hf)-based Copper (Cu) pnictides $HfCu_2X_2$ compounds, this work was designed to identify its fundamental physical and structural characteristics. The $HfCu_2X_2$ compounds are the main component of Zintl family belong to $P\bar{3}m1$ space group having trigonal structure. As far as we are aware, no historical complete data on their various properties are available. The current work contains the brief theoretical calculations of physical properties, by using Wien2k [28] code with (FP-LAPW) potential method to identify various important physical features.

2. Computational parameters

The first principles calculations were taken based on Density functional theory (DFT) [29] within mBJ approximation, the full potential augmented plan waves (FP-LAW) method is implemented in WIEN2K code. To find out the Kohn Sham equation [30], exchange and correlation energy of electrons were handled by using mBJ potential. This is one of the most efficient and reliable method in order to find out the ground state properties based on DFT. To examine the structural relaxation, optimization and also for better understanding of band gap, we performed modified Becke-Johnson exchange potential mBJ. By using Boltzmann transport theory [31], electrical conductivity, electronic thermal conductivity, Seebeck coefficient, electronic transport coefficient can be easily investigated. Furthermore, Boltzmann transport theory of phonons can be used to acquire the lattice thermal conductivity [32]. An acceptable degree of convergence was accomplished by analyzing a number of FP-LAW build functions up to the RMT $K_{max} = 8$. As, K_{max} is the magnitude of the greatest K-vector, and RMT is the slightest radius of the muffin-tin spheres.

3. Results and discussions

3.1. Structure and stability

Our findings show that the trigonal pyramid structure of Hafnium (Hf)-based Copper (Cu) pnictides $HfCu_2X_2$ ($X = N, P, As, Sb, Bi$) has the space group $P\bar{3}m1$ (#164) and the symmetry groups $a = b \neq c$, $\alpha = \beta = 90^\circ$, and $\gamma = 120^\circ$ as demonstrated in Fig. 1. We have optimized the compound structure to study the ground states properties. In the optimized structure, the Hf takes Wyckoff position 1a, while the Cu and the elements X take Wyckoff position 2 d.

The theoretical or calculated lattice constants of all the five compounds were obtained by minimizing the total energy (E_{TOT}) with respect to the lattice parameter [33]. The purpose of optimization is to make a compound stable in order to make our calculation in ground

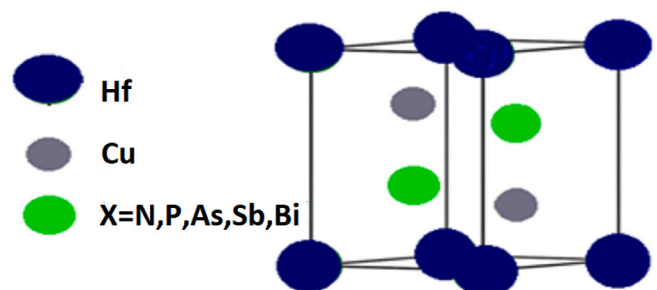


Fig. 1. Relaxed crystal structure of $HfCu_2X_2$ compounds.

state energy. Lattice Parameters value for the optimized structure are noticed in Table 1 and compared with available experimental work [34, 35]. As the anion value shifts from N → Bi, the overall lattice constants (a (Å) and c(Å)) values rise. Such rise in values is due to a change with in atomic size of anions from N → Bi. Both estimated lattice constants and the experimental findings correspond well. The overall reductions from N → Bi in B (GPa) is the confirmation that material compressibility increases as we from top to bottom.

Fig. 2 shows the optimization curve for total energy against volume for all the five reported compounds. To determine the structural and optimized parameters of material, Birch Murnaghan's is used [36]. This equation shows a relation between volume and pressure of body and gives the material energy in relation to volume.

$$E(V) = E_c + \frac{9B_0 V_0}{16} \left\{ \left[\left(\frac{V_0}{V} \right)^{\frac{2}{3}} - 1 \right] B_0 + \left[\left(\frac{V_0}{V} \right)^{\frac{2}{3}} - 1 \right] \left[6 - 4 \left(\frac{V_0}{V} \right)^{\frac{2}{3}} - 1 \right] \right\}$$

3.2. Electronic properties

To understand the material characteristics, electronic band properties is essential feature to recognize the material nature. The electronic properties of HfCu₂X₂ (X = N, P, As, Sb, Bi) type structure is calculated, previously no investigation have been explored for investigating the electronic parameters. We Investigated the electronic band structure, Total and Partial Density of state (TDOS)/(PDOS) for this Zintl phase compound. As seen in Fig. 3(a-e), the compounds band structure display asymmetry lines $\Gamma \rightarrow M \rightarrow K \rightarrow \Gamma \rightarrow A_n$ of the 1st Brillouin zone [37], where K point is considered as most stable point and band gap is the minimum distance that is appeared between conduction band and valence band. There is a valence band (0eV) below the fermi level and a conduction band (0eV) above it.

In case of HfCu₂X₂, the conduction (CB) and valence (VB) single band crosses and overlaps at the fermi level region, which clearly shows its metallic nature with respective potentials [38], clearly observed from Fig. 3(a-e) compounds band structures respectively. As, both conduction and valence band (CB)/(VB) are overlapping with each other in between high symmetry $\Gamma \rightarrow K$ and $\Gamma \rightarrow M$ points. No band gap is appeared in these Zintl phase compounds due to overlapping and missing gap behavior between CB and VB, so it is clear that HfCu₂X₂ compounds show metallic characteristics.

Fig. 4 (a-e) shows the Total Density of State (TDOS) and Partial Density of state (PDOS). Electronic band structure is more endorsed with both states. By means of mBJ potential, Total and Partial Density of states is investigated to get better idea of notable contribution of atoms. Energy distribution of all states can be described via density of state [39].

As, HfCu₂As₂ and HfCu₂Sb₂ for total density of state are calculated from 0 eV to 20 eV energy range. While HfCu₂Bi₂, HfCu₂P₂ and HfCu₂N₂ are investigated from 0 eV to 10 eV energy range. From Fig. 4 (a-e), it is clearly observed that (TDOS) displays a solid acceptance with electronic band properties [40]. The main contribution in total density of state is due to Copper (Cu) atom in all five compounds. In the case of (PDOS), it

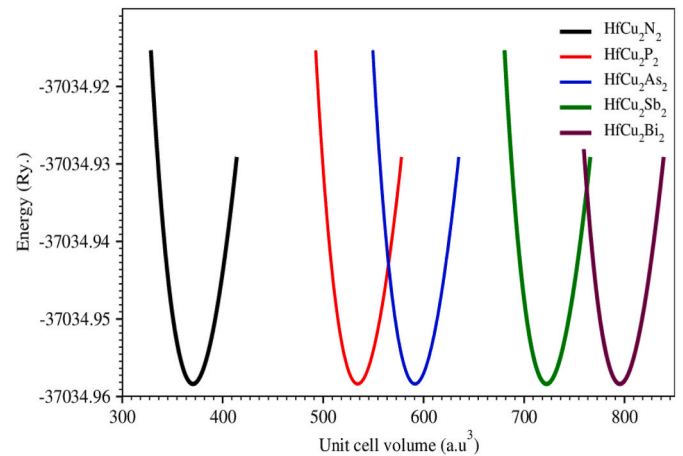


Fig. 2. Optimized plot of energy versus volume for HfCu₂X₂ compounds.

has been demonstrated that in HfCu₂X₂ (X = N, P, As, Sb, Bi), the Cu-d state makes the most significant contribution, followed by the minor contributions of the Hf-d and X-p states. The (PDOS) plots clearly shows that Cu-d states is dominant as compare to all others s, p, f states. While there is very little contribution of Hf-d and X-p states in HfCu₂X₂.

The lower part of V-B (negative energy region (below -3.5 eV)) is the main contribution of (p-states) of X, d-states of Hf and Cu atoms. The other region in the valence band near fermi level at energy ranges from -3 to 0 eV are mainly contributed by d-states of Cu while little contribution of X-p, Hf-d states which is advantageous to electrical transportation in HfCu₂X₂ compounds.

As a moves from N to Bi on the periodic table, the valence/conduction bands stay at the Fermi level due to the metallic nature in each of these compounds. In C-B (positive energy region) the most of the credit goes to Hf-d and X-p states while little contribution by minor peaks and humps of Cu/As/Sb-d states is readily visible. The overall, absent band gap emerge in the understudied compounds as a result of a significant hybridization among Cu-d of valence and (Hf-d and X-p) states of conduction bands which is required for electrical transportation.

3.3. Optical properties

Optical properties supply useful facts about a compound's interior structure. Crystalline materials have a plethora of optical properties, making them an advantageously feasible choice for optoelectronic devices in recent years [41]. Optical houses are closely linked to electron mobility and recombination rate which rely on dielectric function with frequency dependence, such function can be utilized to examine the material's optical characteristics [42]. The ϵ_1 and ϵ_2 respectively show real and imaginary components of the dielectric function. Dielectric characteristic with additionally wave vector response is discover out through the frequency which is alike to the hard interplay of photons that are alive with electrons. Also, it expresses complex machine direct

Table 1

Optimized lattice parameters of HfCu₂X₂ compounds.

Compounds	Lattice parameters				Vo	BP	B (GPa)	Eo (Ry)
	a		c					
	This study	Exp	This study	Exp				
HfCu ₂ N ₂	6.61032	-	10.7348	-	370.3807	5.0594	208.5964	-37034.9583
HfCu ₂ P ₂	7.37	3.799 ^a	11.969	-	538.3535	3.7226	128.3683	-38184.3819
HfCu ₂ As ₂	7.49	-	12.16499	-	594.1255	3.6825	114.9689	-45860.2054
HfCu ₂ Sb ₂	8.187	-	13.2957	-	724.9507	3.6541	88.0734	-62750.1197
HfCu ₂ Bi ₂	7.90	-	12.8	-	798.3734	5.0000	61.2833	-123141.777

^a Ref. [34].

^b Ref. [35].

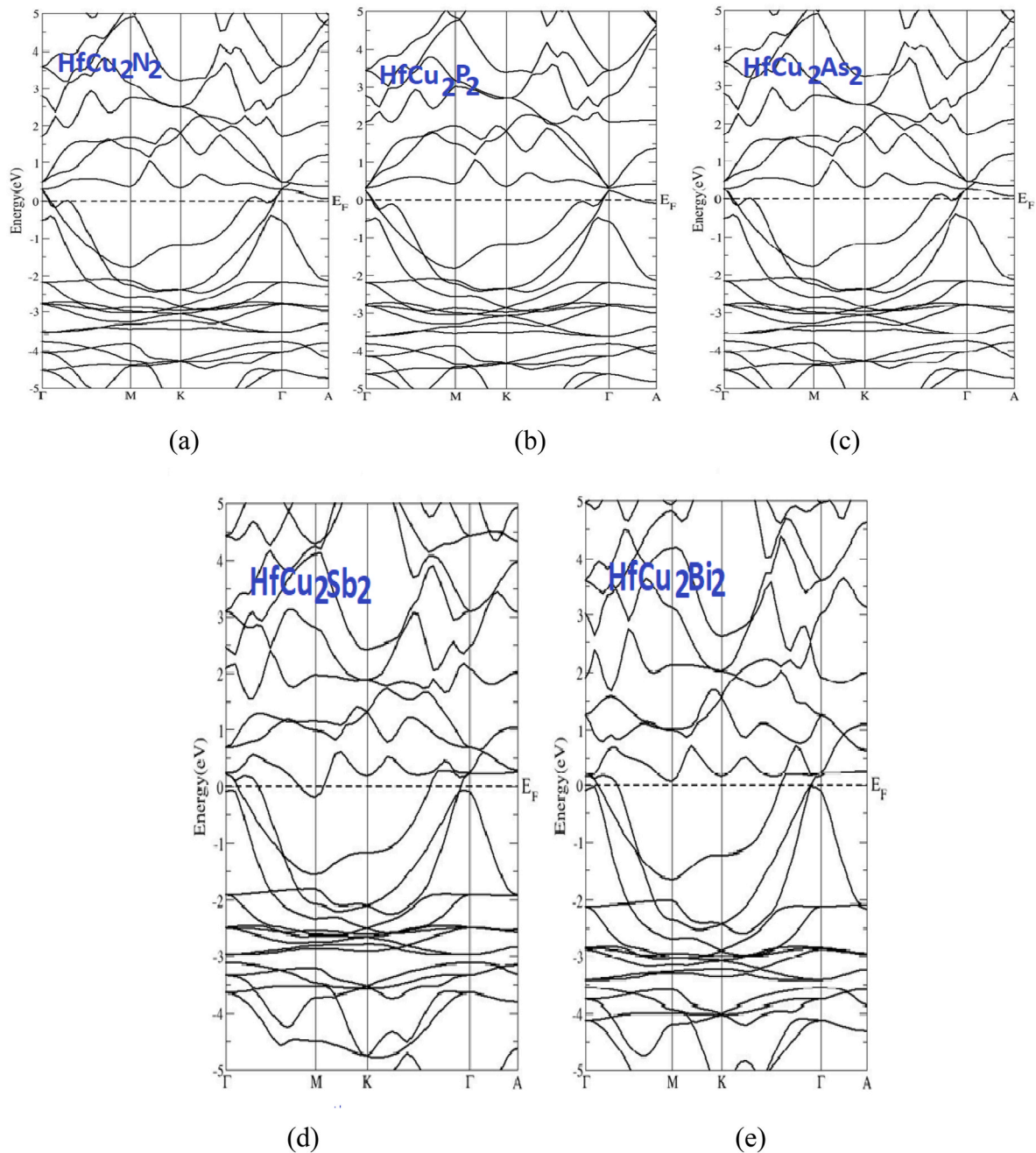


Fig. 3. (A–e) Calculated band structure of HfCu_2X_2 ($X = \text{N, P, As, Sb, Bi}$) with mBJ potential.

response to the active radiation. As, the real/imaginary part of dielectric feature is investigated by the usage of Kramer-kronig relation via the usage of assist of momentum matrix element. The complicated dielectric feature can be determined through given relation.

$$\epsilon_1(\omega) = 1 + \frac{2}{\pi} P \int_0^{\infty} \frac{\omega' \epsilon_2(\omega') d\omega'}{\omega'^2 - \omega^2}$$

$$\epsilon_2(\omega) = \frac{8}{2\pi\omega^2} \sum_{nm'} \left| P_{nm'} \right|^2 \frac{dS_K}{\nabla \omega_{nm'}(K)}$$

Optical parameters of HfCu_2X_2 ($X = \text{N, P, As, Sb, Bi}$) compounds are examined by means of using mBJ potential. Fig. 5 (a) illustrates the real $\epsilon_1(\omega)$ part of dielectric function as a characteristic of power or energy ranging from 0eV to 12eV.

The static function's value of $\epsilon_1(\omega)$ actual phase for HfCu_2N_2 , HfCu_2P_2 , HfCu_2As_2 , HfCu_2Sb_2 , and HfCu_2Bi_2 are 16, 31, 37, 30 and 47 with mBJ respectively. As a result, values of static function's rise when the anion replaced from N \rightarrow Bi. Their values amplify from their static values and gives us first maxima (22.41, 36.94, 42.22, 31.30 and 49.70) at 2.5eV, 1.2eV, 0.9eV, 0.5eV and 1eV with mBJ respectively. The $\epsilon_1(\omega)$ peaks are gradually growing by way of expanding the photon energy. These peaks occur as a consequence of electrons gradually transitioning from the (highest point) top of the valence band to the bottom (lowest point) of the conduction band. The described compounds' primary characteristic peaks are found in the electromagnetic spectrum's infrared-visible energy range.

As the energy level increased, the peaks diminished and descended to their terrible lowest points (below zero) at 5.1eV, 5.3eV, 5.9eV, 4.1eV and 2.4eV with mBJ potential respectively. Additionally, negative

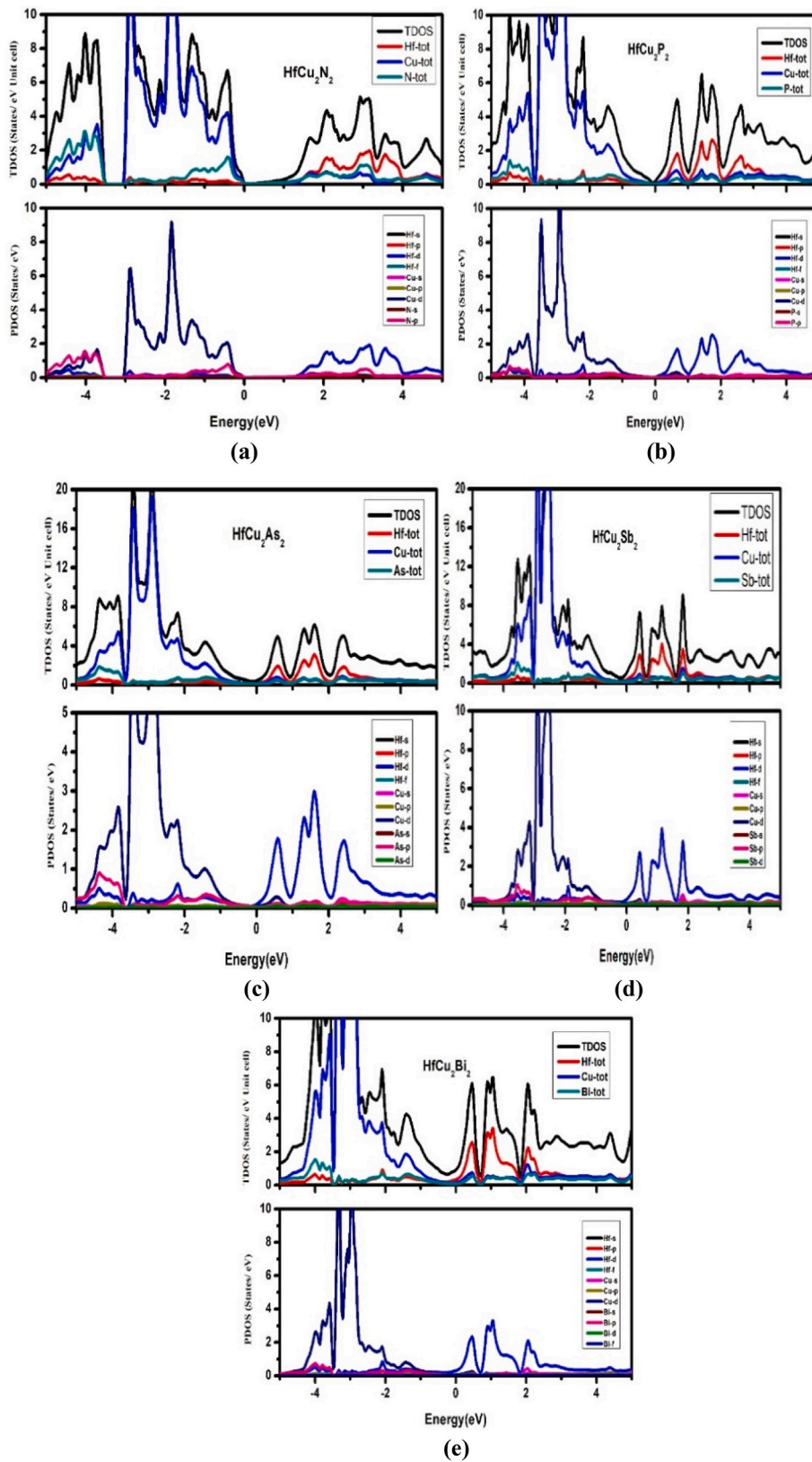


Fig. 4. (A–e) Calculated TDOS and PDOS of HfCu_2X_2 ($X = \text{N, P, As, Sb, Bi}$) with mBJ potential.

values for $\epsilon_1(\omega)$ represent total light attenuation in the optical medium, a material's loss of its dielectric characteristic, and reveal metallic nature. A stage takes place when graphs indicate the constant behavior because of energy loss [43].

In any material case, $\epsilon_2(\omega)$ demonstrates an essential component for optical characteristics. The imaginary part pertaining to energy is shown in Fig. 5(b). By, computing mBJ potential no absorption happens due to the metallic behavior [44] in case of HfCu_2X_2 , absorption condition

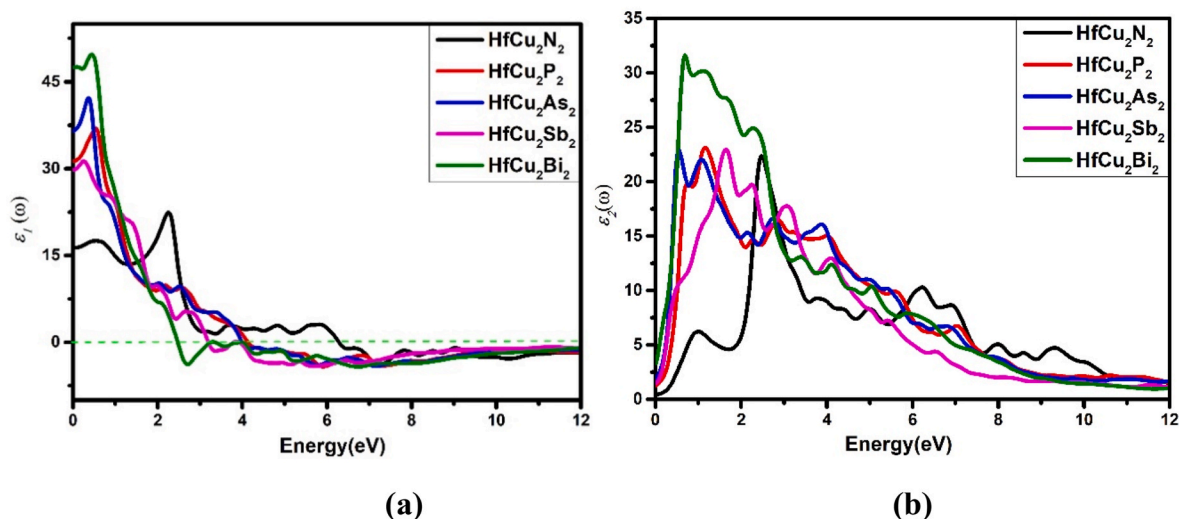


Fig. 5. In a and b the real and imaginary parts of dielectric functions plotted as a function of photon energy (eV) for HfCu_2X_2 with respective mBJ potential.

openly take place perfectly in the material due to the existence as a fact of massive band gap. The non-absorbing standards of HfCu_2X_2 compounds are linked with a zero-band gap. The spectra start at threshold energy with values (0.42, 1.25, 1.91, 1.46 and 3.29) for HfCu_2N_2 , HfCu_2P_2 , HfCu_2As_2 , HfCu_2Sb_2 , and HfCu_2Bi_2 , respectively. These thresholds in the understudied compounds as a result of a significant transition of electrons between Cu-*d* of valence and (Hf-*d* and X-*p*) states of conduction bands.

The curve accelerates significantly further than the threshold points as a result of the combined density of states and transitioning across various orbitals. Each of these compounds have a shoulder around the main peaks. The absorption peaks, though, show larger value of 31.61 for HfCu_2Bi_2 at 0.69 eV and lower value of 22.33 for HfCu_2N_2 at 2.490 eV, thus indicating the dispersion of (*N*-based) compounds throughout the whole UV area.

Additionally, the graphs demonstrate that in the group from $\text{N} \rightarrow \text{Bi}$, the dispersion behavior of HfCu_2X_2 declines. The studied compound's peak is in the visible region, while in a sudden transitioning from $\text{N} \rightarrow \text{Bi}$, it changed towards reduced energy and increased in the infrared visible area. Being a HfCu_2X_2 material with zero bandgap, it has been reported to have a significant absorption that fills the full visible spectrum along with ultraviolet photons. In general, stable and UV-Vis absorbent materials are strong contenders for solar cell manufacturing.

Energy loss as a characteristic of the photon energy from 0 to 12 eV is generally shown in Fig. 6 (a). Fastest shifting of electrons via substance losses their energy is called as loss of energy or Plasmon oscillations. In the case of HfCu_2N_2 , HfCu_2P_2 , HfCu_2As_2 , HfCu_2Sb_2 and HfCu_2Bi_2 topmost peaks (Plasmon peak) in energy loss are considerably located at 12.1 eV, 10eV, 10.2 eV, 11 eV and 11.2 eV for mBJ potential respectively. Plots demonstrate how $\epsilon_1(\omega)$ approaches '0' at such energies. By regular growing the energy loss from photons also grew. These distinguished peaks arise at 0eV for (mBJ) potential.

In Fig. 6 (b) demonstrates reflectivity of HfCu_2X_2 with relation to photon energy from 0 to 12 eV. The variation in the spectra is due to the gradual alteration of peaks; by boosting photon energy, the E-loss increases and reflectivity decreases, and vice-versa [45,46]. The figure makes it obvious that $R(0)$ value (51.3%) for HfCu_2As_2 is higher than the remaining compounds. $R(0)$ values for HfCu_2N_2 , HfCu_2P_2 , HfCu_2As_2 , HfCu_2Sb_2 and HfCu_2Bi_2 is 36.4%, 48.5%, 51.3%, 47.7%, and 47.4% respectively adopt the similar behavior as $\epsilon_1(0)$. The top most reflectivity of HfCu_2N_2 , HfCu_2P_2 , HfCu_2As_2 , HfCu_2Sb_2 and HfCu_2Bi_2 are 55.3% (10.49eV), 55.7% (8.39eV), 57.1% (8.42eV), 56.4% (7.25eV) and 59.9 (8.26eV) respectively. The material's high UV energy range is obtained when reflectivity $R(\omega)$ reaches its highest recorded proportions. Our findings indicate that the materials' high obtaining reflectivity value makes them suitable for employment as shielding materials within

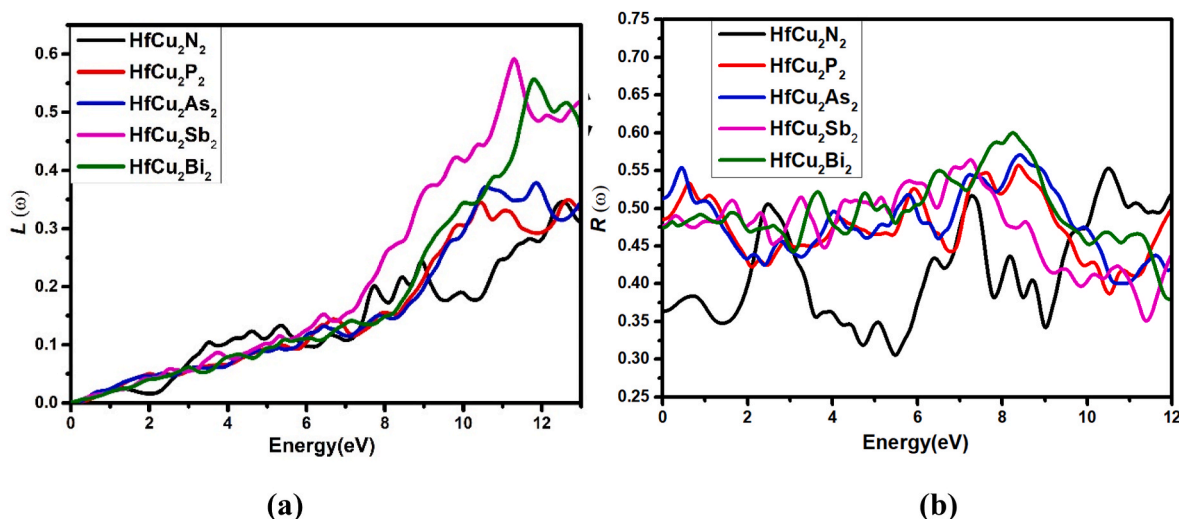


Fig. 6. In a, b calculated the energy loss and reflectivity of dielectric functions as a result of photon energy for HfCu_2X_2 with respective mBJ potential.

range of energies between 3 and 11 eV.

Furthermore, the spectra show that by replacing the anions with $N \rightarrow Bi$, the $R(0)$ overall increases while also broadening the material's high reflectivity range. The reflectivity spectra have a lot of peaks, although the topmost peak and the maximum reflection throughout occur in the $HfCu_2Bi_2$ compound with mBJ potential. Compounds with strong thermoelectric capabilities are generally found in high reflectivity zones and potentially effective in preventing solar heating.

The examined absorption coefficient $\alpha(\omega)$ plot of spectra versus energy from 0 to 12 eV in Fig. 7(a). This characteristic explains how light waves lose intensity as they pass through a material medium. The absorption procedure is initiated by the electronic transitions from VB to CB. The figure shows the energy band gap of the compounds with values 2.32 eV, 1.90 eV, 0.42 eV, 0.39 eV and 0.36 eV for $HfCu_2N_2$, $HfCu_2P_2$, $HfCu_2As_2$, $HfCu_2Sb_2$ and $HfCu_2Bi_2$ respectively marks the beginning of the absorption coefficient. In addition to the beginning points, the $\alpha(\omega)$ progressively grows and obtains their highest point with the minor peaks and shoulders dominantly appearing on the both sides of the spectrum of each of these described compounds in the ultraviolet region. Further evidence that all these materials are excellent absorbers and promising new candidates for high range frequency-energy optical devices [47], particularly in the ultra-violet part of the spectrum, which comes from the fact that the major peaks of the $\alpha(\omega)$ for $HfCu_2X_2$ compounds are dominated at energy ranges from 4.5 to 11 eV. After accomplishing the maximum values, the spectra start decreasing for all Hf-based compounds.

The highest absorption coefficient peaks for $HfCu_2N_2$, $HfCu_2P_2$, $HfCu_2As_2$, $HfCu_2Sb_2$ and $HfCu_2Bi_2$ are $192.81 \times 10^4 \text{cm}^{-1}$, $173.15 \times 10^4 \text{cm}^{-1}$, $170.14 \times 10^4 \text{cm}^{-1}$, $143.26 \times 10^4 \text{cm}^{-1}$ and $169.32 \times 10^4 \text{cm}^{-1}$ respectively. The largest value is found for $HfCu_2N_2$ while the smallest value for $HfCu_2Sb_2$ compound. Inside the electronic band spectrum, such peaks are mostly created by inter band transitions between several high symmetry points. It is further found that the traits peak locations changed to decrease energies with the anion replacement. It is extra fascinating that the compounds show prominent absorption in the visible-ultraviolet energy region.

Fig. 7 (b) exhibit the refractive index $n(\omega)$ of $HfCu_2X_2$ compound. The refractive index is a measure of the density to rarity of a material medium [46] and it is interesting to note that $n(\omega)$ behaves similarly to $\epsilon_1(\omega)$. The accepted theory supports this tendency that is seen in these spectra. The static refractive index of $HfCu_2N_2$, $HfCu_2P_2$, $HfCu_2As_2$, $HfCu_2Sb_2$ and $HfCu_2Bi_2$ are 4.04, 5.59, 6.05, 5.46 and 5.42 with mBJ potential behaves in a similar way as $\epsilon_1(0)$ respectively. The highest peaks (points) of refractive index $n(\omega)$ of $HfCu_2N_2$, $HfCu_2P_2$, $HfCu_2As_2$,

$HfCu_2Sb_2$ and $HfCu_2Bi_2$ are obtaining with values (4.96, 6.16, 6.57, 5.61 and 5.51) at (2.29eV, 0.56eV, 0.39eV, 0.26eV and 0.20eV) with mBJ respectively, that reside in infrared-visible region of EM spectrum.

It is evident that compounds with zero band gaps have high refractive indices as shown by this study. These findings demonstrate that by substituting $N \rightarrow Bi$, the static and maximum refractive index rises, following the same pattern as $\epsilon_1(0)$.

The highest peak values of these Hf-based compounds with the minor hump and shoulder that emerge on the spectra right side begin to progressively decrease after being reached the peak values, the material is unable to absorb more incoming light due to increasing dispersion photon energy. The figures clearly show that these compounds have high refractive indices in the infrared and progressively decline in the low \rightarrow high UV area.

Fig. 8 represents the extension coefficient $\kappa(\omega)$ for the compound $HfCu_2X_2$ with energy ranges from 0 to 12 eV. The value of $\kappa(\omega)$ mostly starts at near the fundamental band gap with threshold energy but in this study, it starts from zero due to the absence (metallic nature) of band gap. At energies exceeding certain limits, the values of $\kappa(\omega)$ steadily increase and reach their highest peak (point) values in the spectra. The maximum peaks of extension coefficient of $HfCu_2N_2$, $HfCu_2P_2$,

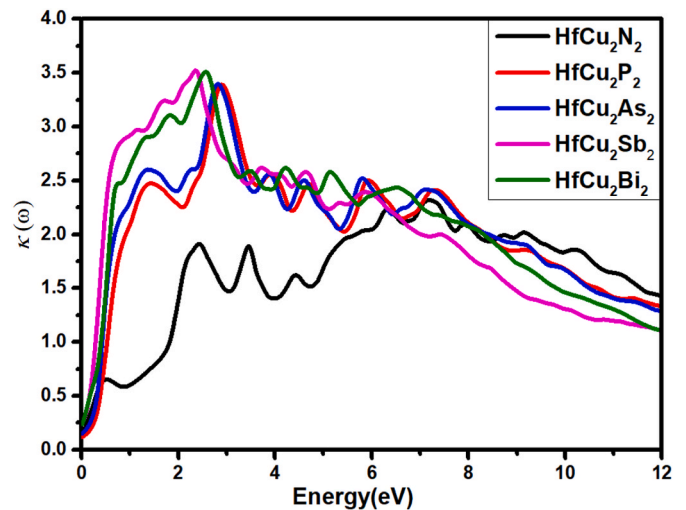


Fig. 8. Calculated extinction coefficient as a result of photon energy for $HfCu_2X_2$ with respective mBJ potential.

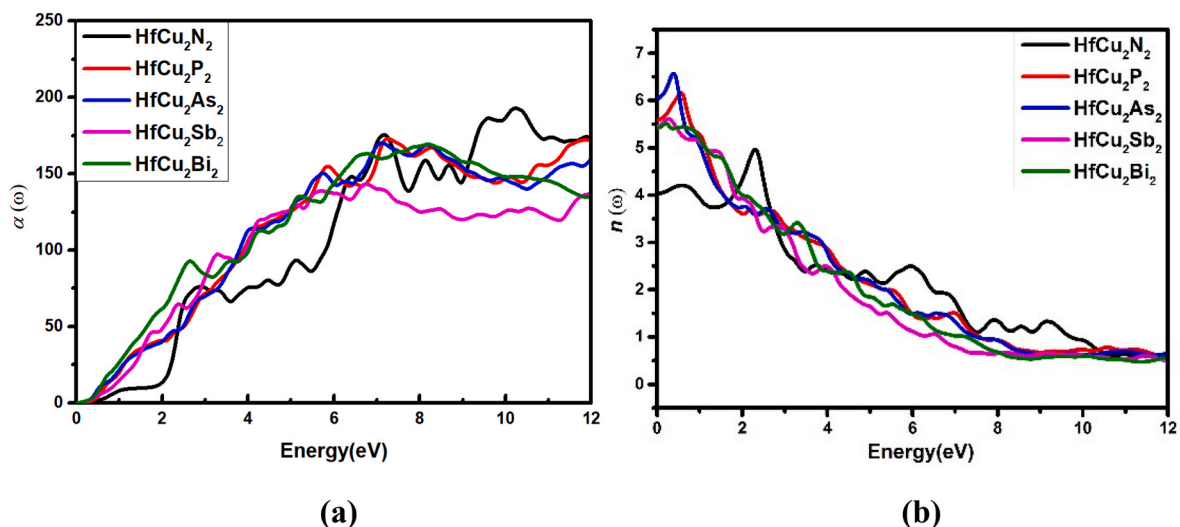


Fig. 7. In a, b Plotted optical conductivity and refractive index of dielectric functions as a result of photon energy for $HfCu_2X_2$ with respective mBJ potential.

HfCu₂As₂, HfCu₂Sb₂ and HfCu₂Bi₂ are obtaining with values (2.32, 3.39, 3.40, 3.52 and 3.51) at (7.19eV, 2.89eV, 2.82eV, 2.35eV and 2.57eV) with mBJ potential respectively. Peak values of $\kappa(\omega)$ exhibit the highest level of absorption behavior. The HfCu₂Sb₂ has the highest extinction coefficient, which indicates that it absorbs more photons than the others.

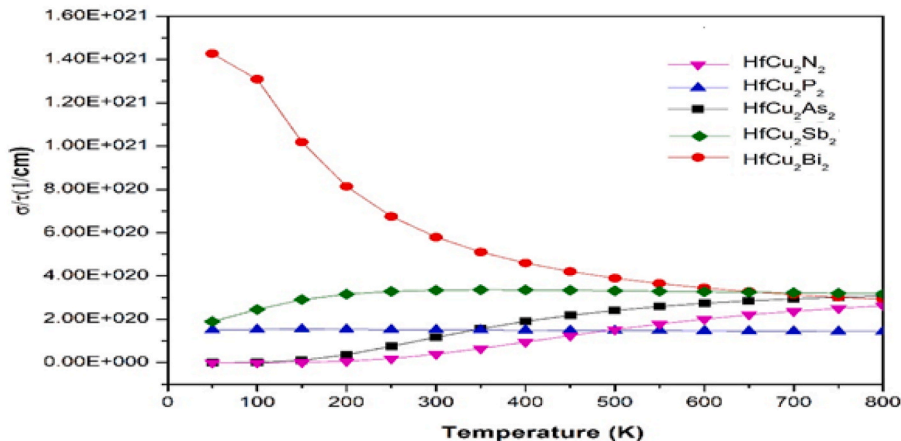
3.4. Thermoelectric properties

In order to maximize the effectiveness of thermal equipment/devices, waste heat energy can be properly converted into useable electrical energy. To improve thermal performance due to electrical conductivity or temperature change (ΔT), thermal conductivity (K) should be minimized and Seebeck coefficient (S) maximized. Temperature depends upon thermal conductivity ($WK^{-1}m^{-1}$), electrical conductivity σ (S/m), and associated Seebeck coefficient (μVK^{-1}). The created (BoltzTrap) software was included in the simulation code [14, 16, 24, 26]. The alliance between electronic band structure, thermal conductivity, and thermoelectric efficiency is genuine. Electrical conductivity and Seebeck coefficient can be measured at the Fermi level using an energy band. A figure of merit is a number that is used to describe how well a technology, system, or approach performs in comparison to its competitors. Research on these kinds of compounds is

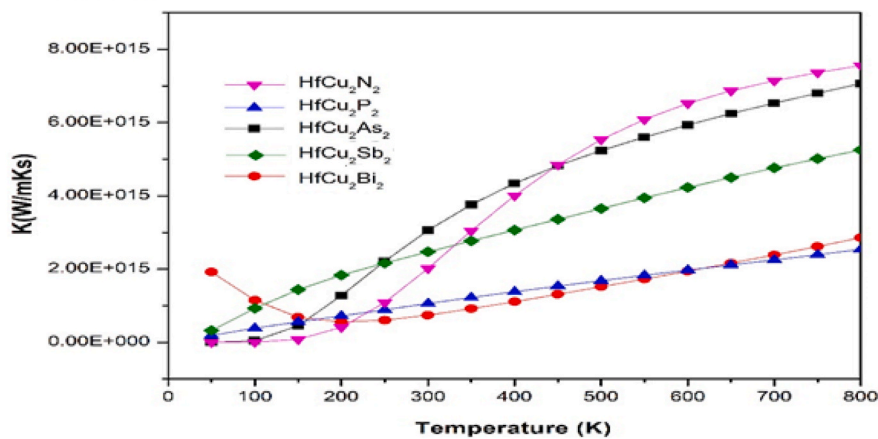
accelerating due to their excellent thermoelectric performance.

Electrical Conductivity has a tremendous impact on the transportation of free carrier of charge, which include in electronic band structure as well as density of state. As evidenced by Fig. 9(a), that moving electrons are responsible for the electrical conductivity [48]. By using mBJ potential it can be observed that HfCu₂P₂ remain constant and shows no increment in the values of electrical conductivity, by increasing temperature it remains constant from 500 K to 800 K temperature range. On the other hand, HfCu₂As₂, HfCu₂Sb₂ and HfCu₂N₂ are increasing and shows their maximum electrical conductivity throughout their complete temperature range. While HfCu₂Bi₂ shows decrement in electrical conductivity and attained lowest value at 800 K. As, electrons can migrate from a high to a low temperature zone in thermoelectric devices due to obtaining extra thermal energy at maximum temperature.

Fig. 9(b), represents the temperature-dependent thermal conductivity (K). In accordance with Fourier's law, $g = -K\Delta T$ shows thermal conductivity. Where g represent the heat flux and K is constant which is accurate for less difference in temperature. As, changing in temperature produce thermal conductivity, depend upon the free charge carrier. In conductors and metals heat conversion is mainly take place by free electrons. In case of HfCu₂X₂ the minimum temperature set for thermal conductivity is 50 K. In the given figure, thermal conductivity increases



(a)



(b)

Fig. 9. In (a), calculated electrical conductivity and in (b) calculated thermal conductivity as a result of temperature (K) for HfCu₂X₂ with mBJ potentials respectively.

when temperature increases from 50 K to 800 K. As, it is shown in Fig. 9 (b), that HfCu_2N_2 , HfCu_2P_2 , HfCu_2As_2 and HfCu_2Sb_2 showing increase in value of thermal conductivity with increase in temperature. While in case of HfCu_2Bi_2 , thermal conductivity decreases until 200 K and then gradually rise in the value is measured [49].

Fig. 10(a) displays the comparison between Seebeck coefficient and temperature. Seebeck coefficient S (μVK^{-1}) steadily determine the induced thermoelectric voltage in response to a temperature change. It can be seen that from Fig. 10(a), there is no change in seebeck coefficient [51] curves of HfCu_2Sb_2 and HfCu_2P_2 still remain at zero over the whole temperature spectrum, while seebeck coefficient of HfCu_2Bi_2 is slightly increase from its negative values at 50 K–200 K and then stood at zero within a given range of temperature. Further, in case of HfCu_2As_2 , seebeck coefficient curves in the negative region (n-type) is significantly increase within 50–550 K temperature range and then gradually move toward zero. While, the seebeck coefficient curve of HfCu_2Bi_2 in the positive region (p-type) is gradually decreasing from 50 to 550 K and then shows constant behavior till 800 K temperature. From Fig. 10(a), it is evident that each of the five compounds has not change curves and shows steady behavior after a specific range of temperature.

Fig. 10(b), shows the values of Power factor [50] of zintl phase compound HfCu_2X_2 ($X = \text{N}, \text{P}, \text{As}, \text{Sb}, \text{Bi}$). The range of temperature is taken from 50 K to 800 K. From Fig. 10(b), it is observed that the values of the power factor of HfCu_2As_2 start increasing from 100 K to 250 K then gradually start decreasing and reaches its minimum value at 800 K. While Power factor (P.E) value of HfCu_2Bi_2 continuously decreasing its values and reaches zero at 250 K and then increasing over the entire temperature range. On the other hand, HfCu_2P_2 , HfCu_2N_2 and HfCu_2Sb_2 values of Power factor (P.E) are gradually increasing and decreasing

from 50 K to 800 K. As, HfCu_2As_2 and HfCu_2Bi_2 reaches maximum Power factor (P.E) values around 800 K.

Fig. 11, represents the (ZT) as compared to the temperature range. The figure of merit (ZT) was accustomed to find out the thermoelectric response of material. The material that shows high figure of merit values is considered highly effective as compare to other materials. In this Fig. 11, it can be seen that HfCu_2As_2 compound shows higher value of (ZT) that is 1.1 followed by HfCu_2N_2 and HfCu_2Bi_2 with values (1 and 0.9) at 50 K temperature. The curve of ZT of HfCu_2As_2 gradually decreases with increasing temperature, whereas that of HfCu_2N_2 and HfCu_2Bi_2 decreases abruptly and shows its minimum values at 800 K. The ZT curves for HfCu_2Sb_2 and HfCu_2P_2 compounds start at the lowest value and exhibit very little and no change through the studied temperature range. In comparison to other compounds, HfCu_2As_2 , HfCu_2N_2 and HfCu_2Bi_2 are considered sufficient and promising materials for thermoelectric devices because they have a maximum ZT value and also because the ZT curves decrease with growing temperature and reach a minimum value of zero at 800 K.

4. Conclusion

In this study, we investigated the structural, optoelectronic and thermal properties of HfCu_2X_2 ($X = \text{N}, \text{P}, \text{As}, \text{Sb}, \text{Bi}$) by using Density functional theory (DFT) at mBJ potential. Following Zintl family compound gives zero band gap, showing that HfCu_2X_2 have metallic characteristics in nature due to overlapping in between high symmetry $\Gamma \rightarrow \text{K}$ and $\Gamma \rightarrow \text{M}$ points between conduction and valence band. The optical parameters are examined within energy range from 0 to 12eV. The maximum reflection occurs in HfCu_2Bi_2 compound, while HfCu_2Sb_2

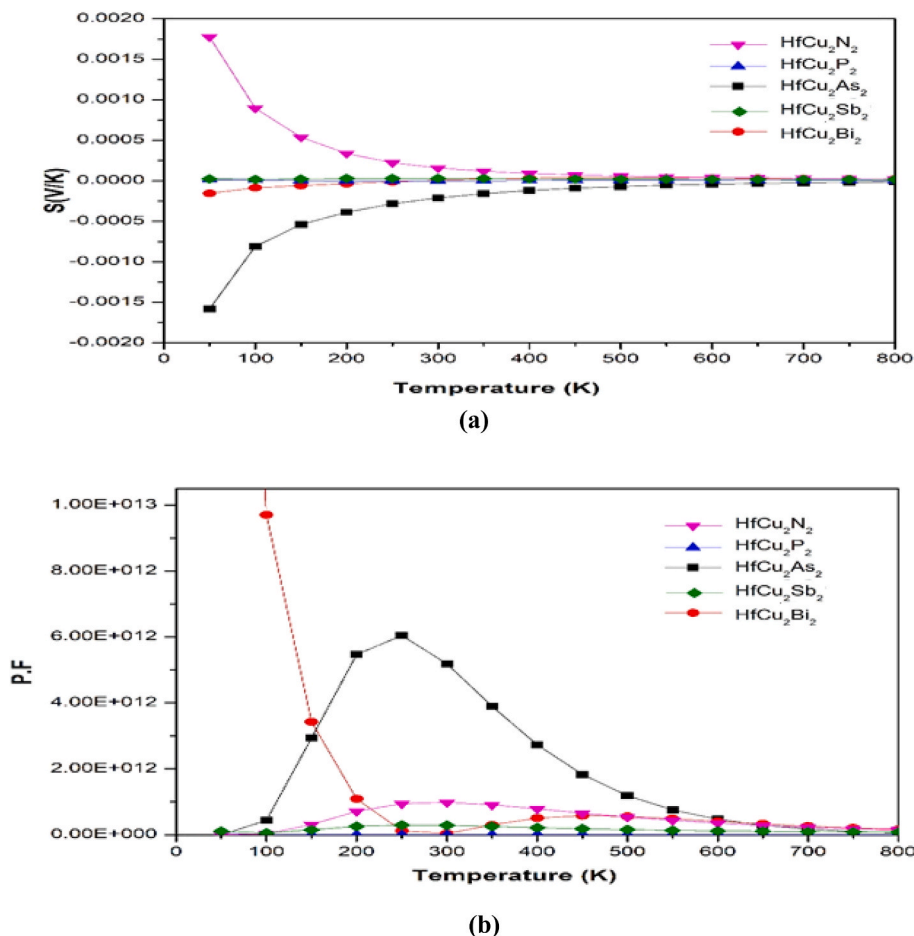


Fig. 10. In (a) calculated seebeck coefficient and in (b) calculated power factor with respect to temperature (K) for HfCu_2X_2 with mBJ potentials respectively.

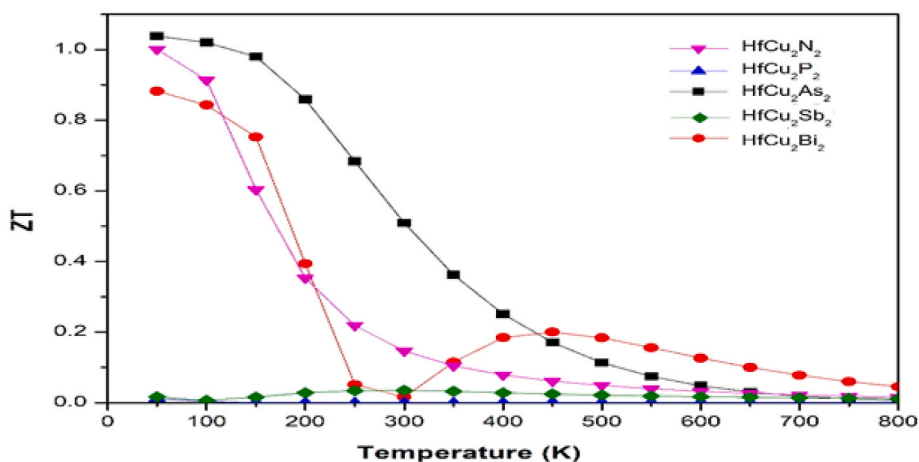


Fig. 11. Calculated dimensionless ZT with respect to temperature (K) for HfCu_2X_2 with mBJ potentials respectively.

achieved the highest extinction coefficient. This is the further evidence that overall, these materials are excellent absorbers and promising new candidates for high range frequency-energy optical devices. By using BoltzTrap codes, thermoelectric response of the Hf-based materials is plotted in relation to temperature. It is evident that HfCu_2As_2 compound shows higher value of ZT that is 1.1. Furthermore, the compound HfCu_2As_2 depicts (n-type) while HfCu_2Bi_2 shows (p-type) nature within 50–550 K temperature range. Depend on the investigation's facts these materials with strong thermoelectric capabilities are most promising candidates for the potentially effective optical and thermoelectric innovations.

Declaration of competing interest

The authors declare that they have no known competing financial interests or personal relationships that could have appeared to influence the work reported in this paper.

Data availability

No data was used for the research described in the article.

Acknowledgments

This research project (for A. Laref) was supported by a grant from the "Research centre of the Female Scientific and Medical Colleges", Deanship of Scientific Research, King Saud University.

References

- Z. Zada, R. Zada, A.A. Khan, M. Saqib, M.F.U. Rehman, M. Ismail, M. Faizan, Investigation of electronic structure, magnetic stability, spin coupling, and thermodynamic properties of novel antiferromagnets XMn_2Y_2 (X= Ca, Sr; Y= P, As), *J. Mol. Struct.* 1268 (2022), 133698.
- Y.P. Feng, L. Shen, M. Yang, A. Wang, M. Zeng, Q. Wu, C.R. Chang, Prospects of spintronics based on 2D materials, *Wiley Interdiscip. Rev. Comput. Mol. Sci.* 7 (5) (2017) e1313.
- K. Fatima, Q. Ain, L. Mohammed, M. Jamil, A.M. Khan, M. Yousaf, J. Munir, Ground state electronic structure, optical and thermoelectric response of Zintl phase MgAl_2X_2 (X= C, Sb) for renewable energy applications, *Phys. B Condens. Matter* 631 (2022), 413688.
- S.Q. Xia, S. Bobev, Are $\text{Ba}_{11}\text{Cd}_6\text{Sb}_{12}$ and $\text{Sr}_{11}\text{Cd}_6\text{Sb}_{12}$ Zintl phases or not? A density-functional theory study, *J. Comput. Chem.* 29 (13) (2008) 2125–2133.
- H.A. Alburaih, S. Aman, S. Mehmood, Z. Ali, S.R. Ejaz, R.Y. Khosa, H.M.T. Farid, First principle study of opto-electronic and thermoelectric properties of Zintl Phase XIn_2Z_2 (X= Ca, Sr and Z= As, Sb), *Appl. Phys. A* 128 (5) (2022) 1–13.
- J. Munir, A.S. Jbara, Q. Ain, K. Fatima, N.A. Noor, H. Naeem, M. Yousaf, An insight into the electronic, optical and transport properties of promising Zintl-phase BaMg_2P_2 , *Phys. B Condens. Matter* 618 (2021), 413181.
- M.W. Iqbal, M. Manzoor, H. Ateeq, S. Azam, G. Murtaza, S. Aftab, A. Majid, Structural, electronic, optoelectronic and transport properties of LuZnCuAs_2 compound: first principle calculations under DFT, *Phys. B Condens. Matter* 596 (2020), 412351.
- Z.M. Elqahatani, S. Aman, S. Mehmood, Z. Ali, A. Hussanan, N. Ahmad, H.M. T. Farid, n-Type narrow band gap A_3InAs_3 (A= Sr and Eu) Zintl phase semiconductors for optoelectronic and thermoelectric applications, *J. Taibah Univ. Sci.* 16 (1) (2022) 660–669.
- Z. Zhang, Y. Yan, X. Li, X. Wang, J. Li, C. Chen, Q. Zhang, A dual role by incorporation of magnesium in YbZn_2Sb_2 Zintl phase for enhanced thermoelectric performance, *Adv. Energy Mater.* 10 (29) (2020), 2001229.
- Z. Zada, A.A. Khan, A.H. Reshak, S. Zada, M. Ismail, M. Fazal-ur-Rehman, M. M. Ramli, Insight into the electronic structure, magnetic, and thermoelectric properties of transition metal pnictides KCr_2L_2 (K= Ca, Sr; L= P, As): as substitute source for renewing energy, *Phys. B Condens. Matter* 649 (2023), 414470.
- A.A. Khan, M. Saqib, Z. Zada, F. Chahed, M. Ismail, M. Ishaq, M. Faizan, Electronic structure, magnetic, and thermoelectric properties of BaMn_2As_2 compound: a first-principles study, *Phys. Scripta* 97 (6) (2022), 065810.
- Z. Zada, R. Zada, A.A. Khan, M. Saqib, M.F.U. Rehman, M. Ismail, M. Faizan, Investigation of electronic structure, magnetic stability, spin coupling, and thermodynamic properties of novel antiferromagnets XMn_2Y_2 (X= Ca, Sr; Y= P, As), *J. Mol. Struct.* 1268 (2022), 133698.
- A.A. Khan, A.H. Reshak, Z. Zada, M. Saqib, Z. Abbas, M. Ismail, A. Laref, Thermoelectric, structural, electronic, magnetic, and thermodynamic properties of CaZn_2Ge_2 compound, *The European Physical Journal Plus* 137 (3) (2022) 1–12.
- R. Bibi, Z. Zada, A.A. Khan, S. Azam, M. Irfan, B.U. Haq, S.A. Khan, First-principles calculations of structural, electronic, magnetic, thermoelectric, and thermodynamic properties of BaMn_2P_2 in the Anti and ferromagnetic phase, *J. Solid State Chem.* 302 (2021), 122388.
- A.A. Khan, A.H. Reshak, Z. Noor, G. Murtaza, M.M. Al-Anazy, H. Althib, J. Bila, First-principles calculations of structural, electronic, optical, and thermoelectric properties of ternary d-metal sulfides Sc_2CdS_4 and Y_2CdS_4 compounds, *Int. J. Energy Res.* 45 (9) (2021) 13657–13667.
- Z. Zada, H. Ullah, R. Zada, S. Zada, A. Laref, S. Azam, M. Irfan, Structure stability, half metallic ferromagnetism, magneto-electronic and thermoelectric properties of new zintl XCr_2Bi_2 (X= Ca, Sr) compounds for spintronic and renewable energy applications, *Phys. B Condens. Matter* 607 (2021), 412866.
- A.A. Khan, W. Khan, A. Khan, A. Laref, A. Zeb, G. Murtaza, Investigation of the structural, electrical, optical and magnetic properties of $\text{XMg}_4\text{Mn}_6\text{O}_{15}$ (X= K, Rb, and Cs) compounds, *Mater. Res. Express* 6 (6) (2019), 066102.
- A.A. Khan, A.A. Khan, M. Yaseen, A. Laref, N. Ullah, I. ur Rahman, The effect of replacing pnictogen elements on the physical properties SrMg_2 (X= P, As, Sb, Bi) Zintl compounds, *Chin. Phys. B* 27 (4) (2018), 047102.
- J. Hwang, H. Kim, D. Wijethunge, N. Nandihalli, Y. Eom, H. Park, W. Kim, More than half reduction in price per watt of thermoelectric device without increasing the thermoelectric figure of merit of materials, *Appl. Energy* 205 (2017) 1459–1466.
- A.A. Khan, A.U. Rehman, A. Laref, M. Yousaf, G. Murtaza, Structural, optoelectronic and thermoelectric properties of ternary CaBe_2X_2 (X= N, P, As, Sb, Bi) compounds, *Z. Naturforsch.* 73 (10) (2018) 965–973.
- A.A. Khan, M. Yaseen, A. Laref, G. Murtaza, Impact of anion replacement on the optoelectronic and thermoelectric properties of CaMg_2X_2 , X=(N, P, As, Sb, Bi) compounds, *Phys. B Condens. Matter* 541 (2018) 24–31.
- H.J. Goldsmid, Bismuth telluride and its alloys as materials for thermoelectric generation, *Materials* 7 (4) (2014) 2577–2592.
- J.F. Li, W.S. Liu, L.D. Zhao, M. Zhou, High-performance nanostructured thermoelectric materials, *NPG Asia Mater.* 2 (4) (2010) 152–158.
- G. Murtaza, A.A. Khan, M.M. Al-Anazy, A. Laref, Q. Mahmood, Z. Zada, M. Aman, Anionic variations for BaMg_2X_2 (X= N to Bi) compounds by density functional theory, *The European Physical Journal Plus* 136 (2) (2021) 1–16.
- L.D. Zhao, D. Berardan, Y.L. Pei, C. Byl, L. Pinsard-Gaudart, N. Dragoie, Bi 1–x Sr x CuSeO oxytelurides as promising thermoelectric materials, *Appl. Phys. Lett.* 97 (9) (2010), 092118.

- [26] A.A. Khan, R. Hasil, A. Laref, N. Ullah, M. Sajjad, A. Zeb, G. Murtaza, DFT prediction of the structural, electronic, thermoelectric and optical properties of ternary pnictides MgBe₂X₂ (X= N, P, As, Sb, Bi): a novel analysis of beryllium with 2A-and 5B-Elements of the structure type CaAl₂Si₂, Solid State Commun. 300 (2019), 113667.
- [27] Z. Zada, H. Ullah, R. Zada, A.A. Khan, A. Mahmood, S.M. Ramay, Electronic band profiles, magnetic stability, antiferromagnetic spins ordering and thermodynamics properties of novel antiferromagnet CaCr₂Sb₂, The European Physical Journal Plus 136 (4) (2021) 1–12.
- [28] P. Blaha, An Augmented Plane Wave+ Local Orbitals Program for Calculating Crystal Properties, wien2k, 2001.
- [29] S.A. Tawfik, O. Isayev, C. Stampfl, J. Shapter, D.A. Winkler, M.J. Ford, Efficient prediction of structural and electronic properties of hybrid 2D materials using complementary DFT and machine learning approaches, Advanced Theory and Simulations 2 (1) (2019), 1800128.
- [30] R. Bauernschmitt, R. Ahlrichs, Stability analysis for solutions of the closed shell Kohn–Sham equation, J. Chem. Phys. 104 (22) (1996) 9047–9052.
- [31] S. Park, S. Woo, E.J. Mele, H. Min, Semiclassical Boltzmann transport theory for multi-Weyl semimetals, Phys. Rev. B 95 (16) (2017), 161113.
- [32] J.A. Cooley, P. Promkhan, S. Gangopadhyay, D. Donadio, W.E. Pickett, B.R. Ortiz, S.M. Kauzlarich, High seebeck coefficient and unusually low thermal conductivity near ambient temperatures in layered compound Yb_{2-x}Eu_xCdSb₂, Chem. Mater. 30 (2) (2017) 484–493.
- [33] C.W. Tucker Jr., J.B. Sampson, Interstitial content of radiation-damaged metals from precision X-ray lattice parameter measurements I. Principles of the measurements, Acta Metall. 2 (3) (1954) 433–438.
- [34] Y.F. Lomnitskaya, ZrCu₂P₂ and HfCu₂P₂ phosphides and their crystal structure, Zhurnal neorganicheskoy himii 31 (1) (1986) 72–74.
- [35] H. Namiki, M. Murase, T. Sasakawa, Single crystal growth and magnetic transport properties of layered transition metal pnictides (Zr/Hf) Cu₂P₂, in: Proceedings of the Physical Society of Japan vol. 74, The Physical Society of Japan, 2019, 1 (pp. 1410–1410).
- [36] T. Katsura, Y. Tange, A simple derivation of the Birch–Murnaghan equations of state (EOSs) and comparison with EOSs derived from other definitions of finite strain, Minerals 9 (12) (2019) 745.
- [37] H. Peelaers, C.G. Van de Walle, Brillouin zone and band structure of β-Ga₂O₃, Phys. Status Solidi 252 (4) (2015) 828–832.
- [38] A. Slepko, A.A. Demkov, First-principles study of Zintl aluminide SrAl₂, Phys. Rev. B 85 (19) (2012), 195462.
- [39] A. Khireddine, A. Bouhemadou, S. Alnujaim, N. Guechi, S. Bin-Omran, Y. Al-Douri, A.K. Kushwaha, First-principles predictions of the structural, electronic, optical and elastic properties of the zintl-phases AE₃GaAs₃ (AE= Sr, Ba), Solid State Sci. 114 (2021), 106563.
- [40] N. Guechi, A. Bouhemadou, Y. Medkour, Y. Al-Douri, R. Khenata, S. Bin-Omran, Electronic and thermoelectric properties of the layered Zintl phase CaIn₂P₂: first-principles calculations, Phil. Mag. 100 (23) (2020) 3023–3039.
- [41] B.U. Haq, A. Afaq, G. Abdellatif, R. Ahmed, S. Naseem, R. Khenata, First principles study of scandium nitride and yttrium nitride alloy system: prospective material for optoelectronics, Superlattice. Microst. 85 (2015) 24–33.
- [42] A. Betal, J. Bera, S. Sahu, Low-temperature thermoelectric behavior and impressive optoelectronic properties of two-dimensional X₁₂ (X= Sn, Si): a first principle study, Comput. Mater. Sci. 186 (2021), 109977.
- [43] A. Lawal, A. Shaari, R. Ahmed, N. Jarkoni, Sb₂Te₃ crystal a potential absorber material for broadband photodetector: a first-principles study, Results Phys. 7 (2017) 2302–2310.
- [44] Q. Mahmood, M. Hassan, Systematic first principle study of physical properties of Cd_{0.75}Ti_{0.25}Z (Z= S, Se, Te) magnetic semiconductors using mBJ functional, J. Alloys Compd. 704 (2017) 659–675.
- [45] S.R. Thahirunnisa, I.B. Shameem Banu, Optical properties of novel ASiP₂ (A= Ca, Sr) chalcopyrites: first-principle study, Appl. Phys. A 124 (12) (2018) 1–7.
- [46] D.D. Sang, Q.L. Wang, C. Han, K. Chen, Y.W. Pan, Electronic and optical properties of lithium niobate under high pressure: a first-principles study, Chin. Phys. B 24 (7) (2015), 077104.
- [47] M.J.I. Khan, J. Liu, S. Hussain, M.N. Usmani, M.I. Khan, A.U.R. Khalid, First principle study of optical properties of Cu doped zincblende GaN for novel optoelectronic applications, Optik 208 (2020), 164529.
- [48] A. Bekhti-Siad, K. Bettine, D.P. Rai, Y. Al-Douri, X. Wang, R. Khenata, C.H. Voon, Electronic, optical and thermoelectric investigations of Zintl phase AE₃AlAs₃ (AE= Sr, Ba): first-principles calculations, Chin. J. Phys. 56 (3) (2018) 870–879.
- [49] H. Usui, K. Kuroki, First principles study on the thermoelectric performance of CaAl₂Si₂-type Zintl phase compounds, J. Phys. Soc. Jpn. 89 (12) (2020), 124707.
- [50] T. Pandey, A.K. Singh, High thermopower and ultra low thermal conductivity in Cd-based Zintl phase compounds, Phys. Chem. Chem. Phys. 17 (26) (2015) 16917–16926.
- [51] L. Xi, J. Yang, L. Wu, J. Yang, W. Zhang, Band engineering and rational design of high-performance thermoelectric materials by first-principles, Journal of Materiomics 2 (2) (2016) 114–130.